Advances in Radiation Oncology (2023) 8, 101267

advances in radiation oncology

www.advancesradonc.org

Original Report

Early in vivo Radiation Damage Quantification for Pediatric Craniospinal Irradiation Using Longitudinal MRI for Intensity Modulated Proton Therapy

Chih-Wei Chang, PhD,[a] Matt Goette, PhD,[a] Nadja Kadom, MD,[b] Yinan Wang, MD,[a] Jacob Wynne, MD,[a] Tonghe Wang, PhD,[c] Tian Liu, PhD,[d] Natia Esiashvili, MD,[a] Jun Zhou, PhD,[a] Bree R. Eaton, MD,[a,*] and Xiaofeng Yang, PhD[a,*]

[a]Department of Radiation Oncology and Winship Cancer Institute, Emory University, Atlanta, Georgia; [b]Department of Radiology and Imaging Sciences, Emory University and Children's Healthcare of Atlanta, Atlanta, Georgia; [c]Department of Medical Physics, Memorial Sloan Kettering Cancer Center, New York, New York; and [d]Department of Radiation Oncology, Mount Sinai Medical Center, New York, New York

Received 19 January 2023; accepted 28 April 2023

Purpose: Proton vertebral body sparing craniospinal irradiation (CSI) treats the thecal sac while avoiding the anterior vertebral bodies in an effort to reduce myelosuppression and growth inhibition. However, robust treatment planning needs to compensate for proton range uncertainty, which contributes unwanted doses within the vertebral bodies. This work aimed to develop an early in vivo radiation damage quantification method using longitudinal magnetic resonance (MR) scans to quantify the dose effect during fractionated CSI.

Methods and Materials: Ten pediatric patients were enrolled in a prospective clinical trial of proton vertebral body sparing CSI, in which they received 23.4 to 36 Gy. Monte Carlo robust planning was used, with spinal clinical target volumes defined as the thecal sac and neural foramina. T1/T2-weighted MR scans were acquired before, during, and after treatments to detect a transition from hematopoietic to less metabolically active fatty marrow. MR signal intensity histograms at each time point were analyzed and fitted by multi-Gaussian models to quantify radiation damage.

Results: Fatty marrow filtration was observed in MR images as early as the fifth fraction of treatment. Maximum radiation-induced marrow damage occurred 40 to 50 days from the treatment start, followed by marrow regeneration. The mean damage ratios were 0.23, 0.41, 0.59, and 0.54, corresponding to 10, 20, 40, and 60 days from the treatment start.

Conclusions: We demonstrated a noninvasive method for identifying early vertebral marrow damage based on radiation-induced fatty marrow replacement. The proposed method can be potentially used to quantify the quality of CSI vertebral sparing and preserve metabolically active hematopoietic bone marrow.

Sources of support: This study was partly supported by the National Institutes of Health (Award Numbers R01CA215718, R01EB032680, P30CA138292, and P30CA008748).

Research data are stored in an institutional repository and will be shared upon request to the corresponding author.

*Corresponding authors: Bree R. Eaton, MD; and Xiaofeng Yang, PhD; E-mails: brupper@emory.edu xiaofeng.yang@emory.edu

https://doi.org/10.1016/j.adro.2023.101267

Introduction

Craniospinal irradiation (CSI) is a curative treatment for several pediatric central nervous system malignancies. The CSI target volume includes the entire brain and thecal sac as the clinical target volume (CTV) to minimize the risk of tumor dissemination throughout the neuroaxis.[1] Conventional photon CSI treatment may induce various short- and long-term side effects, including odynophagia, anorexia, bone marrow suppression causing lymphopenia, and secondary malignant neoplasms[2-5] in these young patients, who have very favorable prognoses. Clinical evidence also has shown that growing children can further develop spinal lordosis, kyphosis, or scoliosis when growth plates are asymmetrically irradiated.[6-8] Consequently, pediatric radiation oncologists have historically recommended treating vertebral bodies and growth plates holistically for growing children.[9] Even with this practice, Paulino et al[10] reported that 16.7% and 54.5% of patients developed scoliosis 15 years after their vertebral ossification centers received CSI doses of 18-24 Gy and 34.2-40 Gy, respectively. Thus, a treatment technique with conformal dose delivery and avoidance of the vertebral bodies is desired for CSI in children to reduce toxicity and improve quality of life.

Intensity modulated proton therapy[11] is an attractive technique for the treatment of pediatric central nervous system malignancies, owing to its superior dose conformality and reduced integral dose to surrounding healthy tissues. Clinical evidence has shown that proton CSI can reduce radiation toxicity and achieve equivalent long-term disease control relative to photon therapy.[12-15] Unlike photon beams, the integral depth dose curve of proton beams exhibits a distal peak near the end of the proton range (Bragg peak) that enables dose deposition without a significant exit dose. Proton CSI has the potential to leverage this physical feature to treat the entire thecal sac while sparing the spinal growth plate. However, current proton therapy treatment planning usually includes a margin of 3.5%, reserved for proton range uncertainty.[16,17] Such uncertainty requires the inclusion of parts of the vertebral bodies during treatment planning to ensure that the target volume receives adequate dose coverage, and the sparing of growth plates can be compromised.

Given this uncertainty in proton therapy, a method of quantifying in vivo proton damage during treatment would be valuable to verify the accuracy of treatments and facilitate adaptive replanning, if necessary, when using a steep dose gradient for vertebral body sparing (VBS). After proton CSI, radiation-induced fatty marrow infiltration can be observed in the spine after treatment, using magnetic resonance imaging (MRI).[18,19] Replacement of hematopoietic marrow provides physiological evidence that supports retrospectively investigating the potential in vivo proton range uncertainty.[20,21] However, there remains a paucity of data from which to deduce when marrow conversion happens and how to use this information to protect vertebral growth plates and increase hematopoietic marrow preservation.

Although fatty marrow replacement has been detected at the end of treatment,[22,23] whether fatty marrow may be observed on magnetic resonance (MR) images between earlier treatment fractions in children remains unknown. This study aimed to perform MRI at specified intervals during proton VBS CSI to determine how early radiographic marrow changes become evident and evaluate whether the planned radiation dose deposition in bone is correlated with proportional proton damage within vertebral marrow. These findings may potentially be used to support real-time medical decision-making—for instance, to determine whether growth plates are sufficiently spared or whether replanning is necessary to reduce excessively conservative proton range margins. Quantification of uncertainty will demonstrate the reliability, applicability, and feasibility of the proposed method for CSI intensity modulated proton therapy with VBS.

Methods and Materials

Patient identification, scan characteristics, and treatment planning

Patients were enrolled in a prospective clinical trial of proton VBS CSI in children with any malignancy, aged less than or equal to 18 years. Patients and their families signed informed consent forms for this institutional review board–approved protocol. Details of the protocol-specified treatment and primary outcomes are separately reported. This work focuses on the secondary endpoint: evaluating the feasibility of using MRI performed during CSI as a method of in vivo quantification of radiation dose deposition to bone marrow.

Patients underwent computed tomography (CT) simulation in the supine position using a 5-point thermoplastic mask for immobilization. CT scans were acquired from the vertex to pelvis using a Siemens SOMATOM Definition Edge scanner with a resolution of $0.98 \times 0.98 \times 1.0$ mm^3. Prescribed doses ranged from 15 to 36 Gy (relative biologic effectiveness [RBE]) in 1.5- to 1.8-Gy (RBE) daily fractions, assuming an RBE of 1.1, per International Atomic Energy Agency/International Commission on Radiation Units and Measurements guidelines.[24,25] The CTV included the entire cranial contents and thecal sac surrounding the spinal cord and nerve roots. The cranium was treated with a single posteroanterior field or 2 posterior oblique fields, and the spinal thecal sac was treated with 1 to 2 posteroanterior fields. Treatment was planned in RayStation using Monte Carlo robust optimization with 5 mm positional and 3.5% range uncertainties.

MRI scans were acquired at baseline (within 6 weeks before starting CSI), during CSI treatment at approximately fractions 7, 13, and 20, and at 4 weeks after completion of treatment. A window of ±3 days was allowed for MRI scans during CSI treatment. MRI sequences included T1- and T2-weighted turbo spin echo MR sequences without contrast acquired in the sagittal plane on a Siemens MAGNETOM Aera 1.5T scanner, with a slice spacing of 0.78 to 4 mm and a pixel spacing of 0.78×0.78 to 1.09×1.09 mm^2. Echo time and repetition time ranges were 10 to 13 ms and 550 to 771 ms for T1-weighted images and 69 to 102 ms and 1500 to 4420 ms for T2-weighted images, respectively. Table 1 summarizes patient demographics and diagnoses as well as imaging and treatment details.

MRI scans during treatment were reviewed by a pediatric neuroradiologist and compared with the baseline image to determine at which earliest time point radiation-induced bone marrow changes could be detected visually. Quantitative image processing was also performed to evaluate radiation-induced bone marrow changes, as described subsequently.

Imaging processing

Varian Velocity was used to register MRI (moving images) to CT (target images). Lumbar spine contours from level L1-L5 were propagated from the CT images to MRI. The lumbar vertebrae were selected for their relatively fixed position relative to other vertebrae, which reduces registration error between imaging modalities. Two-Gaussian distribution sum models were used to analyze MRI intensity within the lumbar contours. Before treatment, bone marrow was intact, and as a result, the MR intensity histogram was reasonably approximated by a single Gaussian distribution. During treatment, irradiated hematopoietic bone marrow is converted to fatty marrow. The 2 marrow types exhibit distinct MR signal intensity such that their intensity histograms show 2 separate Gaussian distributions. Figure 1 shows an example of an MR histogram as a probability distribution after spine irradiation. Equation 1 defines the radiation damage ratio by integrating the area under the total MRI signal distribution curve ($G(x)$) from the intersection point (x_{int}) of the 2 intensity distributions. The variable x is the relative MRI signal intensity. Relative MRI signal is used for analysis to reduce MRI signal discrepancies from each patient. To obtain relative MRI signals for image standardization, we first analyzed each patient's histograms of raw MRI intensity within the vertebral body. The signals in the bottom fifth percentile of the histogram were used for normalization to derive relative MRI intensities for each patient, because the bottom fifth percentile signals were minimally affected by irradiation.

$$\text{Damage ratio} = \int_{x_{int}}^{\infty} G(x)dx \quad (1)$$

Results

Damage ratio variation along with dose to 1% of the volume and time

We evaluated radiation-induced fatty marrow infiltration within the L1-L5 vertebrae for 10 patients using multiple MRIs acquired throughout treatment. Figure 2a1-a2 depicts the proton isodose profile across the region of interest. Of note, parts of the vertebrae received the full prescription dose of 36 Gy (RBE) for patient 1. Figure 2b1-b2 displays the pretreatment T1-weighted MRI and corresponding signal intensity distribution within the lumbar vertebrae as a Gaussian distribution. After treatment began, fatty marrow replacement was observed in both MRI and CT-MRI fusion images, shown

Table 1 Summary of the identified pediatric patients

Patient	Age	Diagnosis	CSI spine dose (Gy)	Dose per fraction (Gy)	MR scans
1	3.8	Atypical teratoid rhabdoid tumor	36	1.8	6
2	9.3	Medulloblastoma	36	1.8	6
3	7.1	Medulloblastoma	36	1.8	6
4	16.6	NGGCT	36	1.8	2
5	15.0	NGGCT	36	1.8	2
6	3.2	Medulloblastoma	36	1.8	6
7	11.1	NGGCT	36	1.8	6
8	10.5	Acute myeloid leukemia	15	1.5	4
9	5.7	Pineoblastoma	36	1.8	5
10	8.5	Medulloblastoma	23.4	1.8	2

Abbreviations: CSI = craniospinal irradiation; MR = magnetic resonance; NGGCT = nongerminoma germ cell tumor.

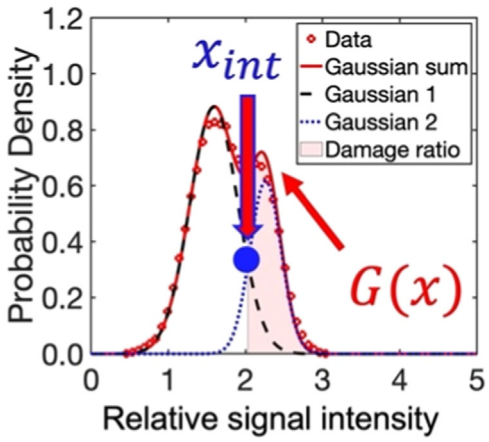

Figure 1 Magnetic resonance histogram presented as a probability density distribution, where x_{int} is the intersection point between Gaussian 1 and Gaussian 2, and $G(x)$ is the total distribution (Gaussian sum).

in Fig. 2c1-f1 and Fig. 2c2-f2. A dose-response relationship was observed for fatty marrow conversion. Figure 2c3 demonstrates that relative MR signal intensity increased after spine irradiation, with a distribution that deviated from a single Gaussian; instead, the new distribution was better approximated by a Gaussian sum composed of 2 Gaussian functions. Figure 2c3 also displays the damaged area (red shadow), which begins at the intersection of the overlapping Gaussian models. By integrating the red area under the Gaussian sum in Fig. 2c3, we found a damage ratio of 0.446 at the 8th fractional dose. Figure 2d3-f3 illustrates the relative MR intensity distributions and damage ratios at different treatment stages.

Figure E1 shows the treatment plan for patient 8. Because the full prescription dose was delivered to portions of the L1-L5 vertebral bodies, fatty marrow conversion was detected in T2-weighted MRIs, displayed in Fig. E1c1-e1. CT-MR fusion images in Fig. E1 depict MR intensity migration with increased dose. Figure E1c3-e3 reveals damage ratios quantified from MR images at different times.

Ultimately, we included data from all patients' MRIs to infer the correlation for the damage ratio variation based on the dose to 1% of the volume (D1 dose) and time. The D1 dose was selected as a figure of merit because this quantity was sensitive to fractional doses. Figure 3a depicts a positive correlation between the damage ratio and D1 dose. Figure 3b shows a quadratic relation between the damage ratio and time with a concave profile, which suggests marrow regeneration after maximal damage.

Dose-signal intensity curve

Figure 4 shows registered MR images exhibiting fatty marrow infiltration at different times with different accumulative doses. Only hematopoietic marrow could be observed before treatments. Fatty marrow started to form only after proton irradiation. As proton accumulative dose increased, the region of fatty marrow increased; the edge of the area aligned well with overlaid isodose lines, which correspond to the distal falloff doses in the vertebral bodies. Figure 4 depicts the dose-response relationship as a function of MR signal intensities. An approximate threshold of 2.25 Gy was observed in these data, and doses increased rapidly with signal intensities. Ultimately, the curve saturated at 34 to 35 Gy.

Discussion

Although fatty marrow replacement has previously been reported after treatment,[20] we used multiple MR scans acquired during treatment to demonstrate an early dose-effect relationship. We observed a correlation between radiation-induced fatty marrow infiltration and D1 dose, and isodose lines aligned to the edge of fatty marrow in vertebral bodies during interfraction treatment.

Figure 3a reveals a steep dose-effect relationship between D1 doses of 15 and 30 Gy, with a decrease in the relative effect thereafter, possibly due to a maximum of accumulated damage acquired during previous fractions. Figure 4 also demonstrates a sharp inflection in the MR signal intensity observed between 2.25 and 34 Gy, with a shoulder region between 34 and 35 Gy (RBE). These observations are consistent with previously published findings indicating the existence of a steep dose-effect correlation in the 15- to 35-Gy range.[26-28] Figure 3b suggests that damage ratios reach a maximum between 40 and 50 days from the start of treatment, with a subsequent decrease, likely representing marrow regeneration, as shown in Fig. 2f1-f2 and corresponding to that reported in a previous study.[23] Meanwhile, the damage ratio shown in Fig. 3b represents the fraction of image voxels with high intensity due to fatty marrow replacement induced by proton irradiation. With the increase in damage ratios, image voxels with strong MRI signals increased, owing to fatty marrow replacement. The decrease in damage ratios indicated that the majority of voxels had low MRI signals, which implies potential bone marrow regeneration after irradiation. The amount of fatty marrow can be potentially used to detect proton range overshooting during interfractional treatment. Such information can support the decision to use adaptive radiation therapy if the range uncertainty is beyond the acceptable tolerance. Because MR data are lacking for cumulative doses of 0 to 10 Gy, Fig. 3 includes an extrapolation region across this range. MR scans acquired with each treatment fraction may reduce uncertainty and further bolster dose-effect correspondence.

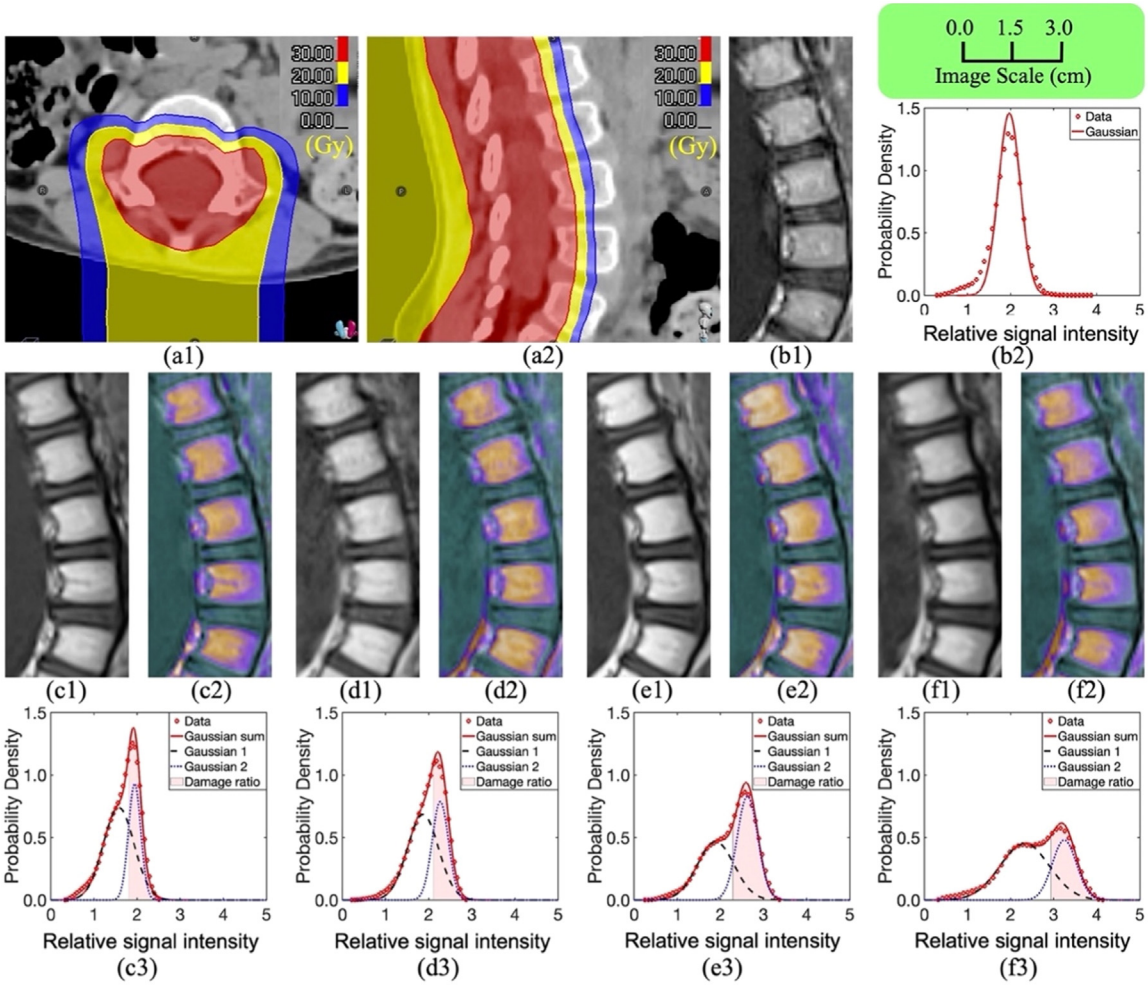

Figure 2 Demonstration of radiation-induced fatty infiltration at the lumbar spine, L1-L5 level, from patient 1, with a prescribed craniospinal irradiation spine dose of 36 Gy in 20 fractions. Radiation therapy treatment planning computed tomography with Monte Carlo dose for (a1) transversal image, L3 level, and (a2) sagittal image. (b1) Sagittal T1-weighted MRI image and (b2) distribution of MRI intensity within vertebral bodies, L1-L5 level, acquired 13 days before the treatment start date. Sagittal T1-weighted MRI images [(c1)/(d1)/(e1)/(f1)], computed tomography–MRI fusion images [(c2)/(d2)/(e2)/(f2)], and distribution of MRI intensity within vertebral bodies, L1-L5 level [(c3)/(d3)/(e3)/(f3)], acquired (c1)-(c3) 15 days (eighth fraction), (d1)-(d3) 26 days (15th fraction), (e1)-(e3) 37 days, and (f1)-(f3) 45 days after the craniospinal irradiation treatment start date. The damage ratios are given by (c3) 0.446, (d3) 0.459, (e3) 0.550, and (f3) 0.392. *Abbreviation:* MRI = magnetic resonance imaging.

Figure 5b-d shows that the distal falloff doses caused fatty marrow replacement in the vertebral bodies and that isodose lines aligned with the edges of fatty marrow. Although the cumulative doses vary in Fig. 5b-d, the quantities of each isodose line do not change significantly, because these isodose lines belong to the distal falloff of the prescription dose regions. Figure 5e shows a decrease in fatty marrow due to potential marrow regeneration such that the marrow edge was pulled back and the edge aligned with a high-dose isodose line. The marrow edge aligned well with the 10-Gy isodose, in agreement with the literature,[29] based on MR images acquired more than 2 months from the treatment start. However, Fig. 5b-d shows that the marrow edges matched isodose lines ranging from 2.25 to 2.88 Gy. The results suggest that MR images acquired during treatments could be used for building dose-and-signal-intensity correlations to avoid biases due to marrow regeneration.

A previous dosimetric study has confirmed fatty marrow conversion with doses as low as 16 Gy.[30] Here, marrow conversion was observed on MRI with doses as low as 2.25 Gy (Fig. 4). Partition growth inhibition and hypoplasia of paraspinal muscles are probable late effects after growing pediatric patients receive proton CSI treatment.[2] The proposed method of early in vivo assessment of radiation damage has the potential to noninvasively confirm adequate VBS while the patient is in treatment. Maintenance of healthy marrow bolsters the patient against the

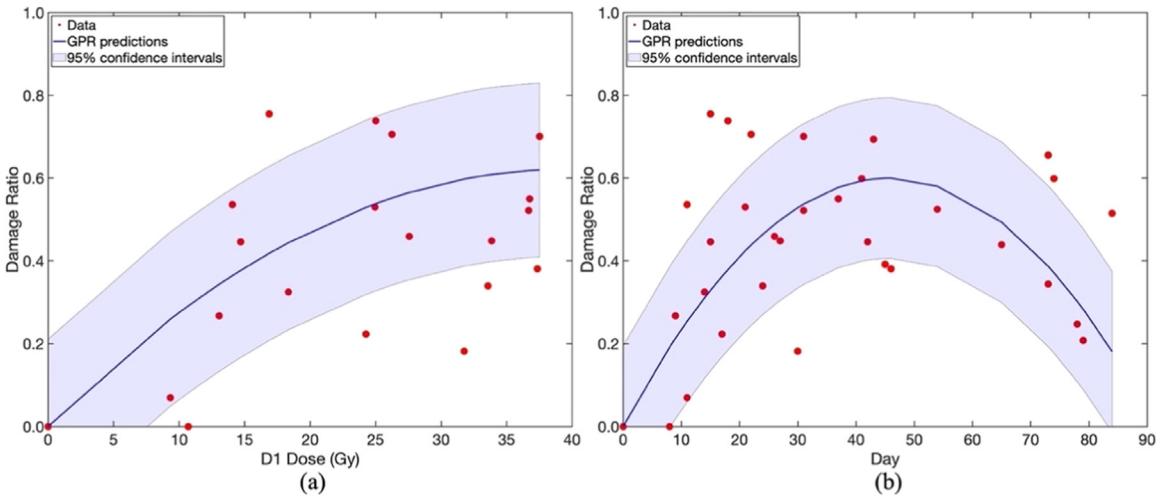

Figure 3 Damage ratio variation along with (a) dose to 1% of the volume and (b) time. Blue lines are predicted by Gaussian process regression, while blue shadows represent 95% confidence intervals.

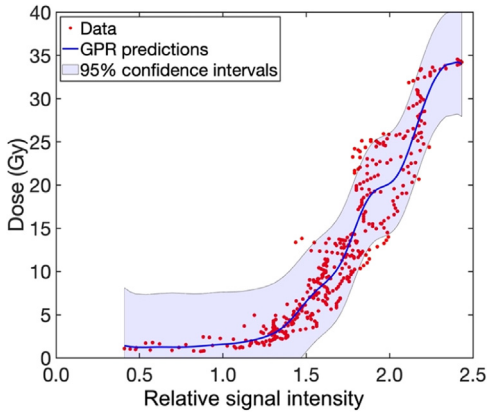

Figure 4 Dose-signal intensity curve (blue line) fitted by GPR using the anteroposterior data points within the vertebra. The blue shadow shows the 95% confidence interval. *Abbreviation:* GPR = Gaussian process regression.

hematologic toxicities of systemic therapy and preserves patient candidacy for any additional treatment that may be required after radiation. Confirmation of VBS further reduces the likelihood of vertebral growth inhibition, which can be a devastating side effect in these patients, who have very favorable prognoses.

The current study only included MR scans sampled between treatment fractions. Owing to this limitation, the sensitivity of MRI signals to fatty marrow could not be quantified, and it remains unclear when fatty marrow replacement happens. Meanwhile, this prospective study was limited in terms of investigating the feasibility of the proposed quantification method for determining radiation damage induced by proton range uncertainty. The accrued clinical effects require a long-term follow-up investigation. The current observations were insufficient to determine the lowest dose that affects growth or bone marrow function. Additionally, this prospective study

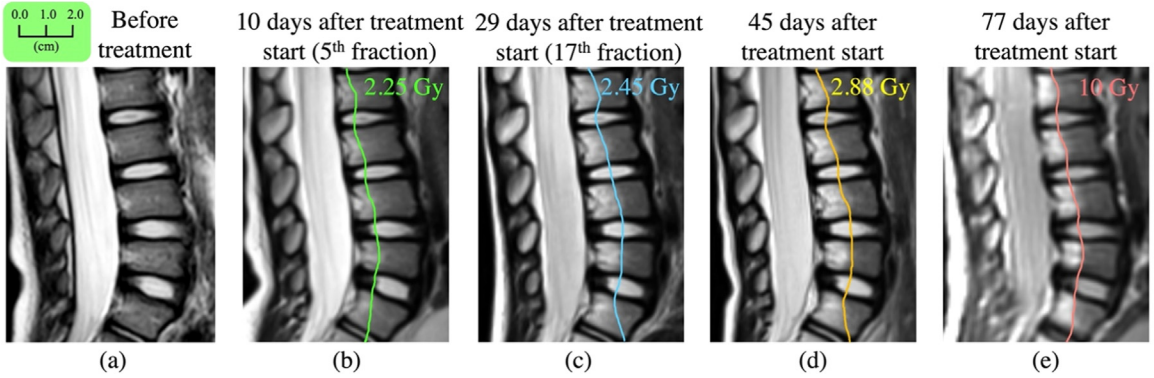

Figure 5 Demonstration of radiation-induced fatty marrow infiltration within the lumbar spine from patient 9. Magnetic resonance images with isodose lines were acquired (a) 42 days before, (b) 10 days after, (c) 29 days after, (d) 45 days after, and (e) 77 days after treatment start.

only focused on the potential effects caused by proton range uncertainty. Growth inhibition can be also caused by a dose falloff over the narrow range distal to the CTV,[9] which falls within the vertebral body. Positional uncertainties, which were accounted for by CTV-based robust optimization planning, also contribute radiation doses to the subarachnoid space, leading to growth issues.[1] It should be emphasized that reducing the proton range uncertainty might not be sufficient to reduce the vertebral dose to a safe margin.

Future investigations may focus on collecting comprehensive MR data for each treatment fraction to more accurately predict when bone marrow suppression occurs. The findings are still in their infancy, and a long-term follow-up investigation is essential to validate the clinical applications. The method presented here may further be integrated with a physics-informed deep learning-based CT material conversion method[31-33] to achieve VBS intensity modulated proton therapy. Such a system would potentially improve treatment plan quality, enable the real-time verification of treatment accuracy, and support medical decision-making for plan modification.

Conclusion

A method for the detection of early in vivo radiation damage is presented that uses serial MR scans to quantify vertebral marrow changes in pediatric CSI patients. The method can identify the transition from hematopoietic marrow to fatty marrow earlier than was previously possible. Such a method can potentially quantify the quality of pediatric proton VBS CSI, with the potential to spare pediatric patients from the most severe toxicities of this essential treatment.

Disclosures

The authors declare that they have no known competing financial interests or personal relationships that could have appeared to influence the work reported in this paper.

Supplementary materials

Supplementary material associated with this article can be found in the online version at doi:10.1016/j.adro.2023.101267.

References

1. Ajithkumar T, Horan G, Padovani L, et al. SIOPE – Brain tumor group consensus guideline on craniospinal target volume delineation for high-precision radiotherapy. *Radiother Oncol*. 2018;128:192-197.
2. Constine LS, Woolf PD, Cann D, et al. Hypothalamic-pituitary dysfunction after radiation for brain tumors. *N Engl J Med*. 1993;328:87-94.
3. Chang EL, Allen P, Wu C, Ater J, Kuttesch J, Maor MH. Acute toxicity and treatment interruption related to electron and photon craniospinal irradiation in pediatric patients treated at the University of Texas M. D. Anderson Cancer Center. *Int J Radiat Oncol Biol Phys*. 2002;52:1008-1016.
4. Packer RJ, Gajjar A, Vezina G, et al. Phase III study of craniospinal radiation therapy followed by adjuvant chemotherapy for newly diagnosed average-risk medulloblastoma. *J Clin Oncol*. 2006;24:4202-4208.
5. Zhang R, Howell RM, Taddei PJ, Giebeler A, Mahajan A, Newhauser WD. A comparative study on the risks of radiogenic second cancers and cardiac mortality in a set of pediatric medulloblastoma patients treated with photon or proton craniospinal irradiation. *Radiother Oncol*. 2014;113:84-88.
6. Paulino AC, Wen BC, Brown CK, et al. Late effects in children treated with radiation therapy for Wilms' tumor. *Int J Radiat Oncol Biol Phys*. 2000;46:1239-1246.
7. Paulino AC, Fowler BZ. Risk factors for scoliosis in children with neuroblastoma. *Int J Radiat Oncol Biol Phys*. 2005;61:865-869.
8. De B, Florez MA, Ludmir EB, et al. Late effects of craniospinal irradiation using electron spinal fields for pediatric cancer patients. *Int J Radiat Oncol Biol Phys*. 2023;115:164-173.
9. Hoeben BA, Carrie C, Timmermann B, et al. Management of vertebral radiotherapy dose in paediatric patients with cancer: Consensus recommendations from the SIOPE radiotherapy working group. *Lancet Oncol*. 2019;20:e155-ee66.
10. Paulino AC, Suzawa HS, Dreyer ZE, Hanania AN, Chintagumpala M, Okcu MF. Scoliosis in children treated with photon craniospinal irradiation for medulloblastoma. *Int J Radiat Oncol Biol Phys*. 2021;109:712-717.
11. Weber DC, Habrand JL, Hoppe BS, et al. Proton therapy for pediatric malignancies: Fact, figures and costs. A joint consensus statement from the pediatric subcommittee of PTCOG, PROS and EPTN. *Radiother Oncol*. 2018;128:44-55.
12. Brown AP, Barney CL, Grosshans DR, et al. Proton beam craniospinal irradiation reduces acute toxicity for adults with medulloblastoma. *Int J Radiat Oncol Biol Phys*. 2013;86:277-284.
13. Eaton BR, Esiashvili N, Kim S, et al. Clinical outcomes among children with standard-risk medulloblastoma treated with proton and photon radiation therapy: A comparison of disease control and overall survival. *Int J Radiat Oncol Biol Phys*. 2016;94:133-138.
14. Farace P, Bizzocchi N, Righetto R, et al. Supine craniospinal irradiation in pediatric patients by proton pencil beam scanning. *Radiother Oncol*. 2017;123:112-118.
15. Huynh M, Marcu LG, Giles E, Short M, Matthews D, Bezak E. Are further studies needed to justify the use of proton therapy for paediatric cancers of the central nervous system? A review of current evidence. *Radiother Oncol*. 2019;133:140-148.
16. Paganetti H. Range uncertainties in proton therapy and the role of Monte Carlo simulations. *Phys Med Biol*. 2012;57:R99-R117.
17. Chang C-W, Huang S, Harms J, et al. A standardized commissioning framework of Monte Carlo dose calculation algorithms for proton pencil beam scanning treatment planning systems. *Med Phys*. 2020;47:1545-1557.
18. Hajek PC, Baker LL, Goobar JE, et al. Focal fat deposition in axial bone marrow: MR characteristics. *Radiology*. 1987;162:245-249.
19. Rosenthal D, Hayes C, Rosen B, Mayo-Smith W, Goodsitt M. Fatty replacement of spinal bone marrow due to radiation: Demonstration by dual energy quantitative CT and MR imaging. *J Comput Assist Tomogr*. 1989;13:463-465.

20. Krejcarek SC, Grant PE, Henson JW, Tarbell NJ, Yock TI. Physiologic and radiographic evidence of the distal edge of the proton beam in craniospinal irradiation. *Int J Radiat Oncol Biol Phys*. 2007;68:646-649.
21. Gensheimer MF, Yock TI, Liebsch NJ, et al. In vivo proton beam range verification using spine MRI changes. *Int J Radiat Oncol Biol Phys*. 2010;78:268-275.
22. Blomlie V, Rofstad EK, Skjønsberg A, Tverå K, Lien HH. Female pelvic bone marrow: Serial MR imaging before, during, and after radiation therapy. *Radiology*. 1995;194:537-543.
23. Cavenagh EC, Weinberger E, Shaw DW, White KS, Geyer JR. Hematopoietic marrow regeneration in pediatric patients undergoing spinal irradiation: MR depiction. *Am J Neuroradiol*. 1995;16:461-467.
24. International Commission on Radiation Units & Measurements (ICRU). ICRU publication 78, prescribing, recording, and reporting proton-beam therapy. Available at: https://www.icru.org/report/prescribing-recording-and-reporting-proton-beam-therapy-icru-report-78/. Accessed December 1, 2007.
25. International Atomic Energy Agency. *Relative Biological Effectiveness in Ion Beam Therapy*. Vienna: International Atomic Energy Agency; 2008.
26. Sonis AL, Tarbell N, Valachovic RW, Gelber R, Schwenn M, Sallan S. Dentofacial development in long-term survivors of acute lymphoblastic leukemia: A comparison of three treatment modalities. *Cancer*. 1990;66:2645-2652.
27. Willman KY, Cox RS, Donaldson SS. Radiation induced height impairment in pediatric Hodgkin's disease. *Int J Radiat Oncol Biol Phys*. 1994;28:85-92.
28. Eifel PJ, Donaldson SS, Thomas PRM. Response of growing bone to irradiation: A proposed late effects scoring system. *Int J Radiat Oncol Biol Phys*. 1995;31:1301-1307.
29. Giantsoudi D, Seco J, Eaton BR, et al. Evaluating intensity modulated proton therapy relative to passive scattering proton therapy for increased vertebral column sparing in craniospinal irradiation in growing pediatric patients. *Int J Radiat Oncol Biol Phys*. 2017;98:37-46.
30. Yankelevitz DF, Henschke CI, Knapp PH, Nisce L, Yi Y, Cahill P. Effect of radiation therapy on thoracic and lumbar bone marrow: Evaluation with MR imaging. *Am J Roentgenol*. 1991;157:87-92.
31. Chang C-W, Dinh NT. Classification of machine learning frameworks for data-driven thermal fluid models. *Int J Therm Sci*. 2019;135:559-579.
32. Chang C-W, Gao Y, Wang T, et al. Dual-energy CT based mass density and relative stopping power estimation for proton therapy using physics-informed deep learning. *Phys Med Biol*. 2022;67: 115010.
33. Chang C-W, Zhou S, Gao Y, et al. Validation of a deep learning-based material estimation model for Monte Carlo dose calculation in proton therapy. *Phys Med Biol*. 2022;67: 215004.